Quantum information spreading in random spin chains with topological order

Takahiro Orito [1], Yoshihito Kuno [2], and Ikuo Ichinose [3]

[1]*Graduate School of Advanced Science and Engineering, Hiroshima University, 739-8530, Japan*
[2]*Graduate School of Engineering Science, Akita University, Akita 010-8502, Japan*
[3]*Department of Applied Physics, Nagoya Institute of Technology, Nagoya, 466-8555, Japan*

Quantum information spreading and scrambling in many-body systems attract interest these days. Tripartite mutual information (TMI) based on operator-based entanglement entropy (EE) is an efficient tool for measuring them. In this paper, we study random spin chains that exhibit phase transitions accompanying nontrivial changes in topological properties. In their phase diagrams, there are two types of many-body localized (MBL) states and one thermalized regime intervening these two MBL states. Quench dynamics of the EE and TMI display interesting behaviors, providing an essential perspective concerning the encoding of quantum information. In particular, one of the models is self-dual, but information spreading measured by the TMI does not respect this self-duality. We investigate this phenomenon from the viewpoint of spatial structure of the stabilizers. In general, we find that knowledge of the phase diagram corresponding to the qubit system is useful for understanding the nature of quantum information spreading in that system. The connection between the present paper and random circuit of projective measurements and also topological Majorana quantum memory is remarked upon.

I. INTRODUCTION

Study of many body localization (MBL) is one of the central issues in condensed matter physics [1–4]. In particular, the entanglement property in the bulk for excited states has been investigated and it is verified that its system-size scaling law behaves differently from that of the thermal phase [3,5]. Also, MBL exhibits a nontrivial dynamical aspect for the quenching time evolution of entanglement entropy (EE). In typical MBL phases, for a specific type of initial state, the EE exhibits a logarithmic growth due to the presence of interactions, where particles (or spin) are not transported but the EE gradually spreads into an entire system [6,7]. Various types of the MBL states have been proposed through many theoretical and numerical works, such as spin-glass MBL (SG-MBL) [8,9], MBL induced by quasiperiodic potential [10], topological MBL [8,11–13], MBL emerging in lattice gauge theories [14–16], and various disorder-free MBLs [17–27], etc. However, it is expected that there are still many different types of MBL categories which have not been explored yet. Moreover, the unique spectral and entanglement structures associated with each type of MBL are diverse and study of these detailed structures gives us an insight to understand how quantum information is encoded and stored in MBL regimes. Study of these issues is useful for understanding, deeply encoding, and storing mechanisms of quantum information in localization systems.

In this paper, we study two disordered spin models exhibiting characteristic multiple topological MBL phases. The disordered spin models exhibit rich phase diagrams because of the emergence of different sets of effective stabilizers for each phase, local integrals of motion (LIOMs) [1] in the context of

MBL, and these different sets of stabilizers are noncommutative with each other. The stabilizers in the disordered models respect symmetries of the models and become basic building blocks of the topological order [11,12,28–31]. Furthermore, the spatial structure of the stabilizers influences the bulk entanglement structure in the MBL phases and also degeneracy of the energy spectrum in the whole band [11,12] (related to the presence of gapless edge modes).

One of our target spin models, random transverse field Ising model *at infinite temperature*, was extensively studied recently [13,32–34]. There, the global phase diagram, which includes two types of MBL phases (paramagnetic MBL and SG-MBL phases), was obtained by numerical investigation. In this paper, we shall study detailed properties of these MBL phases such as quenching dynamics of the EE from the viewpoint of duality. Then we employ some quantum information theoretic quantity, and tripartite mutual information (TMI) proposed in Ref. [35] to investigate the topological MBL from the viewpoint of information spreading. As a measure of the scrambling, the out-of-time-ordered correlator (OTOC) was proposed [36,37], and it was applied to some kind of quantum spin models [38–40]. Compared with the OTOC, the TMI is state and operator independent, and it is becoming a benchmark of the quantum information spreading nowadays. In this paper, we shall numerically demonstrate that the system-size dependence of the TMI is valid to identify phase boundaries of the system. Furthermore, we shall study another disordered spin model having two different types of topological MBLs in its phase diagram. We clarify the model's global phase structure by varying the strength of two types of disorders, and observe the bulk information spreading in the whole parameter region. In particular, we show that the bulk structure of the

information spreading in the topological MBLs is captured by using the TMI and also is determined by the spatial structure of the stabilizers in each phase of MBL.

Among the findings in this paper obtained by the numerical calculation, an interesting observation concerns the infinite random criticality (IRC) and Griffiths phase [41–43] in the random transverse field Ising spin chain. This model has been studied for a long time as one of the most important models for understanding random systems. We shall shed light on its physical properties from the viewpoint of quantum information scrambling in this paper. As another interesting observation, by calculation of the TMI, we acquire an important insight into how quantum information in the bulk is encoded in quantum spin chains and how disorder influences quantum information spreading. Calculation of the TMI in the two-site partitioning of the chain reveals that quantum information is encoded in stabilizer qubits in the MBL regimes.

The rest of this paper is organized as follows. In Sec. II, we shall introduce our target two disordered spin models and explain the basic properties of them. We also introduce the TMI and explain its practical calculation methods briefly. In Sec. III, we show the results of the numerical study by means of the exact diagonalization. Detailed discussions on the numerical results are given there to obtain observations explained in the above. Section IV is devoted to discussion and conclusion.

II. MODELS AND TRIPARTITE MUTUAL INFORMATION

In this section, we introduce two types of spin chains and briefly study their phase diagrams. Then we explain the TMI and methods of the practical numerical calculation.

A. Models

The first model describes a self-dual random Ising spin chain, whose Hamiltonian is given as follows:

$$H_{\text{IC}} = \sum_i \left[J_i \sigma_i^x \sigma_{i+1}^x + h_i \sigma_i^z \right] + H_g,$$

$$H_g = g \sum_i \left[\sigma_i^x \sigma_{i+2}^x + \sigma_i^z \sigma_{i+1}^z \right], \tag{1}$$

where σ_i^x, σ_i^z are Pauli matrices residing on site i of the chain, J_i and h_i are random couplings drawn from uniform distributions $[0, W_J]$ and $[0, W_h]$, respectively, and g is a nonnegative coupling constant. By symmetry of the free part of the Hamiltonian, $H_{\text{IC}}|_{g=0}$, $\{J_i\}$ and $\{h_i\}$ can be transformed to positive values, and therefore we have chosen the above parameter region. For the practical calculation, we set $W_J = (W_h)^{-1} = W$ and introduce a parameter such as $\delta = 2 \ln W = \overline{\ln W_J} - \overline{\ln W_h}$. We are interested in the phase diagram of the system H_{IC} [Eqs. (1)] in the $(\delta - g)$ plane.

It is easily verified that the system H_{IC} has $\mathbb{Z}_2$ symmetry by $\mathbb{P} \equiv \prod_i \sigma_i^z$, and it is also self-dual by the following duality transformation:

$$\tau_i^z = \sigma_i^x \sigma_{i+1}^x, \quad \tau_i^x = \prod_{j \leqslant i} \sigma_j^z, \tag{2}$$

and under Eqs. (2), $\delta \rightarrow -\delta$. The above properties of H_{IC} play an important role in the subsequent investigation of

quantum information spreading in that model. Also, for large W, the model can be regarded as a projective Hamiltonian with effective stabilizers, i.e., LIOMs in the localization literature. These are a set of dimers $\{\sigma_i^x \sigma_{i+1}^x\}$, each of which approximately commutes with H_{IC}, $[\sigma_i^x \sigma_{i+1}^x, H_{\text{IC}}] \approx 0$ for any i. The presence of the stabilizers gives an insight into the bulk property of information spreading [44].

In this paper, we are interested in the system H_{IC} at infinite temperature. A phase diagram of that system has been obtained recently [32], and there exist three phases in the phase diagram, i.e., a paramagnetic MBL phase (PM-MBL) for $\delta < \delta_{1c}$, an ergodic regime for $\delta_{1c} < \delta < \delta_{2c}$, and a MBL phase with a spin-glass/topological order (SG-MBL) for $\delta_{2c} < \delta$. Values of the criticality δ_{1c}, δ_{2c} depend on the strength of the coupling g, and $\delta_{2c} = -\delta_{1c} \equiv \delta_c$ by duality. For the pure transverse random Ising model (TRIM) at $g = 0$, $\delta_c = 0$ showing IRC as in the ground state [41]. For the infinite-temperature system, detailed investigation of the EE and gap ratio for small g by using the system-size dependence and scaling indicates the possibility of an intermediate ergodic phase in a finite δ region such as $-\ln 2 < \delta < \ln 2$ in the limit $g \rightarrow 0$ [32]. This result supports the avalanche picture of the localization-delocalization transition. It is a very interesting problem if the avalanche picture emerges in dynamics of quantum information spreading. We shall comment on this after studying the TMI, which is a benchmark of the scrambling.

In Fig. 1(a), we show the numerical calculations of the half-chain EE for energy eigenstates of H_{IC} for $g = 0.2$, which is defined as follows:

$$\text{EE}^{(s)} = -\text{Tr}_A \left[\rho_r^{(s)} \log(\rho_r^{(s)}) \right], \quad \rho_r^{(s)} = \text{Tr}_{\bar{A}} [|\psi_s\rangle \langle \psi_s|],$$

$$\overline{\text{EE}} = \text{average of EE}^{(s)} \text{ over states and randomness,}$$

where the suffix (s) denotes the combined label of sample number and state label, A and $\bar{A}$ are the half chain and its complement, respectively. (Hereafter, log denotes $\log_2$.) The calculations exhibit the critical value $\delta_c \simeq 2.0$ for $g = 0.2$. The EE has a nonvanishing value $\sim \log 2$ for the deep SG-MBL regime, whereas it reduces to very small in the deep PM-MBL. This result indicates that in the deep SG-MBL, cat states of a parity pair emerge there such as

$$\frac{1}{\sqrt{2}} (|\uparrow\uparrow\downarrow\downarrow \cdots\rangle \pm |\downarrow\downarrow\uparrow\uparrow \cdots\rangle)$$

in the σ^x basis, and then the reduced density matrix ρ_R^{sg} is obtained as

$$\rho_R^{\text{sg}} = \tfrac{1}{2} (|\uparrow\uparrow\downarrow\downarrow \cdots\rangle \langle\uparrow\uparrow\downarrow\downarrow \cdots| + |\downarrow\downarrow\uparrow\uparrow \cdots\rangle \langle\downarrow\downarrow\uparrow\uparrow \cdots|),$$

which gives $\log 2$ for the EE.

The above observation implies the possibility that a pair of states $(|\uparrow\uparrow\downarrow\downarrow \cdots\rangle, |\downarrow\downarrow\uparrow\uparrow \cdots\rangle)$ form a bulk qubit and quantum information is encoded in them. This qubit scrambles information across the system, but initial information is preserved in the wave function in the SG-MBL phase. How robustly this picture of the bulk qubit holds in the unitary time evolution by the Hamiltonian, H_{IC}, is an interesting problem. On the other hand, for random circuits of stabilizers, we think that the bulk qubit is a good picture during time evolution.

Here we emphasize that the Pauli spins at the edges of the open boundary chain with the length L, $\sigma_{1(L)}^x$, commute with
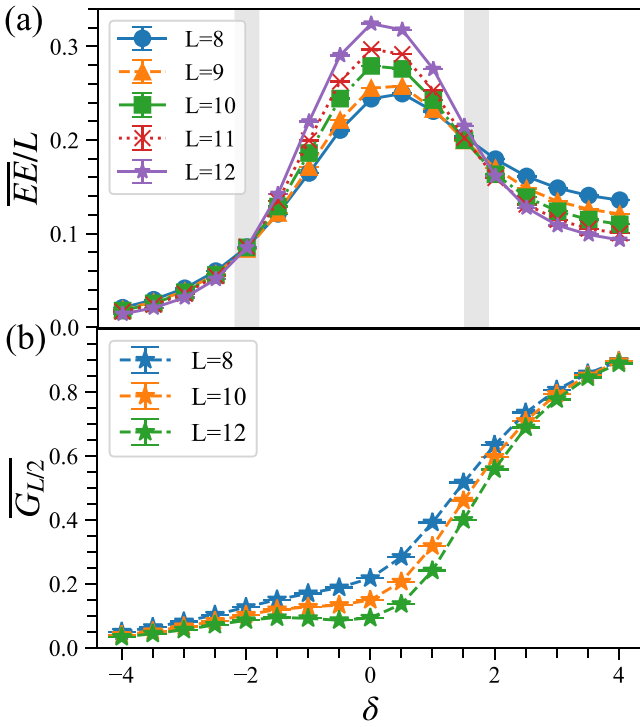
FIG. 1. (a) Half-chain EE for the Ising spin chain model H_{IC} in Eqs. (1) for $g = 0.2$. Calculation of $\overline{\mathrm{EE}}/L$ indicates the existence of two phase transitions such as the PM-MBL $\rightarrow$ ETH $\rightarrow$ SG-MBL as δ increases. As δ is getting large, $\overline{\mathrm{EE}} \rightarrow \log 2$, corresponding to the SG order. These results were obtained by averaging over 1000, 750, 500, 300, and 150 disorder realizations using all eigenstates for the $L = 8, 9, 10, 11, 12$ systems. (b) Spin correlation, $\overline{G}_{L/2}$, in Eq. (3), as a function of δ. Its increase indicates the SG order for $\delta \gg 1$. These results were obtained by averaging over the 20 000 eigenstates using 10–20 eigenstates in the middle of the spectrum at each disorder realization for the $L = 8, 10,$ and 12 systems. The error bars are standard error.

the noninteracting part of the SG-MBL Hamiltonian with $h_i = 0$, $\sum_i J_i \sigma_i^x \sigma_{i+1}^x$, and anticommute with $\mathbb{P}$. Then, $\sigma_{1(L)}^x$ is a zero mode operator from the viewpoint of topological order [45]. The operation of $\sigma_{1(L)}^x$ on the above two cat states interchanges them, respecting $\mathbf{Z}_2$ parity symmetry $\mathbb{P}$. Even for finite $\{h_i\}$, the zero-mode operator can be constructed perturbatively [45], such as $\sigma_1^x + \frac{h_1}{J_1}\sigma_1^z \sigma_2^x + \frac{h_1 h_2}{J_1 J_2}\sigma_1^z \sigma_2^z \sigma_3^x + \cdots$. (In the Majorana representation, gapless edge mode $\gamma_1 = \sigma_1^x$.) Further, this zero mode can survive even in the presence of a finite interaction g, and its explicit form is obtained perturbatively such as [46] $\sigma_1^x + \frac{h_1}{J_1}\sigma_1^z \sigma_2^x + \frac{g}{J_2}\sigma_1^y \sigma_2^y \sigma_3^x + \cdots$.

To verify the property of the phases furthermore, we explore the spin-glass order by studying the spin correlation, $G_{r=L/2}$, defined by [47]

$$G_r = \frac{1}{L - r} \sum_{i=1}^{L-r} \left| \sigma_i^x \sigma_{i+r}^x \right|. \quad (3)$$

The result shown in Fig. 1(b) indicates that the spin-glass order emerges as δ increases from δ_c, as we expect.

The second spin-chain system, which we call an extended random cluster spin (CS) chain [11], is described by the

following Hamiltonian:

$$H_{\mathrm{CS}} = \sum_i \left[J_i \sigma_i^x \sigma_{i+1}^x + \lambda_i \sigma_{i-1}^x \sigma_i^z \sigma_{i+1}^x + \tilde{h}_i \sigma_i^z \right] + H_g, \quad (4)$$

where $\tilde{h}_i$'s are small random variables drawn from $[0, 1]$, and λ_i are uniform random variables drawn from $[0, W_\lambda]$. We define $W_J = (W_\lambda)^{-1} = W$ and also $\delta = 2 \ln W$ as before. As we showed in the above, for sufficiently large W_J, all states in H_{CS} belong to the SG-MBL. On the other hand, for sufficiently large W_λ, H_{CS} approaches the random CS model, which is a symmetry-protected topological (SPT) system with $\mathbb{Z}_2 \times \mathbb{Z}_2$ symmetry [48]. Also, a similar disordered model has been studied and its ground state phase diagram has been clarified in terms of the disorder-strength parameter space [49], where the SPT phase is characterized by the number of the zero-energy Majorana edge modes. It is also known that energy eigenstates of the genuine CS model with only second terms of Eq. (4) are all localized as dictated by LIOMs, $\{\sigma_{i-1}^x \sigma_i^z \sigma_{i+1}^x\}$, and we shall verify in the subsequent calculation that this localization nature remains for small but finite values of $\{J_i\}$. Here, we again emphasize that the above LIOMs are nothing but stabilizers in quantum information theory [28]. Since the single stabilizer takes two eigenvalues ± 1, the operator can be regarded as a logical spin operators, that is, a qubit. In what follows, we call them stabilizer qubits. In the random Ising spin chain with $W \gg 1$, the stabilizer qubits are $\{\sigma_i^x \sigma_{i+1}^x\}$. The stabilizer qubit is one of the key concepts for understanding findings in the present paper as we explain. In contrast to general LIOMs in the conventional MBL, stabilizer qubit realizes localization with some order, e.g., SG or topological order.

To obtain the phase diagram of the system H_{CS} in Eq. (4), we first investigate the half-chain EE and display the numerical calculations in Fig. 2(a). The results show that there are three phases, i.e., two MBL phases and one thermal phase. Interestingly enough, for $\delta \ll -1$, the EE approaches $\log 4$ instead of $\log 2$, although in the presence of the J_i terms as well as the g terms, the Hamiltonian H_{CS} has only $\mathbb{Z}_2$ symmetry. To verify the topological properties of the phase, we calculate a string order, defined as $\mathcal{O}_{\mathrm{st}}(i, j) \equiv \langle \sigma_i^x \sigma_{i+1}^y (\prod_{k=i+2}^{j-2} \sigma_k^z) \sigma_{j-1}^y \sigma_j^x \rangle$. The results of the string order averaged over the randomness, $\Phi_{\mathrm{st}} \equiv \overline{\mathcal{O}_{\mathrm{st}}^2}$, are displayed in Fig. 2(b), which indicate that the topological order corresponding to the genuine CS model exists for $\delta \ll -1$. This is an unexpected result since the finite J_i terms reduce the symmetry from $\mathbb{Z}_2 \times \mathbb{Z}_2$ to $\mathbb{Z}_2$. However, a similar result is observed for the ground state in Ref. [30]. In the clean system, Φ_{st} for the excited state vanishes as expected from the observation in Ref. [8].

In Fig. 2(b), we also show the calculations of the spin-glass order parameter, $G_{L/2}$. We find a similar behavior to that in the random Ising spin chain in Fig. 1(b). That is, a finite value of $G_{L/2}$ for $\delta > 2$ indicates the existence of the spin-glass order, and this result is obviously in good agreement with the EE in Fig. 2(a).

We investigated the infinite-temperature phase diagram of the $g = 0$ system of H_{CS} in Eq. (4). Similarly to the random Ising spin chain, the calculation of the EE seems to indicate the direct transition from the SG-MBL to the CS-MBL. We
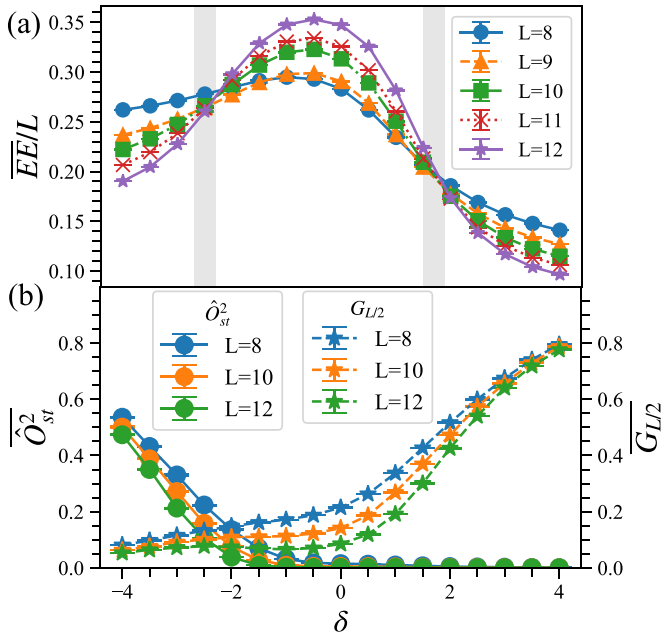
FIG. 2. (a) Half-chain EE for the cluster-spin chain model H_{CS} in Eq. (4) for $g = 0.2$. Calculation of $\overline{EE}/L$ indicates the existence of two phase transitions such as the CS-MBL $\to$ ETH $\to$ SG-MBL as δ increases. As δ is getting large, $\overline{EE} \to \log 2$, corresponding to the SG order, whereas as δ decreases, $\overline{EE} \to \log 4$, coming from emergent $\mathbb{Z}_2 \times \mathbb{Z}_2$ symmetry. These results were obtained by averaging over 1000, 750, 500, 300, and 150 disorder realizations using all eigenstates for the $L = 8, 9, 10, 11, 12$ systems. (b) Spin correlation, $G_{L/2}$ in Eq. (3), as a function of δ. Its increase indicates the SG order for $\delta \gg 1$. On the other hand, the string order, Φ_{st}, acquires nonvanishing values for $\delta < -2$, indicating topological order with $\mathbb{Z}_2 \times \mathbb{Z}_2$ symmetry. These results were obtained by averaging over the 20 000 eigenstates using 10–20 eigenstates in the middle of the spectrum at each disorder realization for the $L = 8, 10,$ and 12 systems.

recently investigated a very close model to H_{CS} in Eq. (4) by using a Majorana fermion [50]. Similar methods can be applied to the model H_{CS} with $g = 0$. (Please see later discussion in Sec. III D.) The model reduces to a random-hopping and random-potential free Majorana fermion, which is similar to the TRIM case [41] and is expected to exhibit a phase transition via varying the strength of the random hopping and potential.

B. Tripartite mutual information

In the previous section, the half-chain EE, spin-glass and string orders identified the MBL phases and thermal phase in the models. Next, we investigate the property of information spreading in each phase. We observe how the information spreading takes place in each phase and how strongly the time-evolution operator works as a scrambler. To quantify the information spreading ability in the system, we employ the TMI, which is a very efficient tool to evaluate the scramble ability of the unitary time evolution operator of the system, as proposed in Ref. [35]. There are already some observations of the TMI in an interacting model and conventional MBL systems [51–55]. In addition, the observation of the TMI can
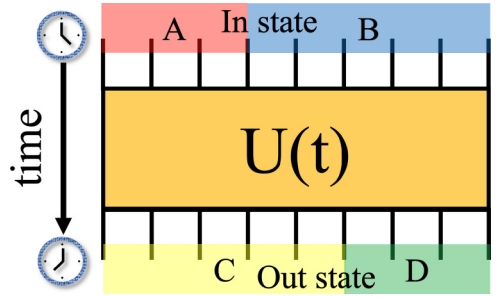

FIG. 3. Schematic image of the time evolution of the state with doubled Hilbert space. The spatial partitioning of the system is represented where four subsystems A–D are introduced.

be an efficient indicator to characterize a phase transition (phase boundary) in the context of the measurement-induced phase transition [56].

Let us explain the TMI and the practical methods of the numerical calculation [55] to be applied for the target models with L lattice sites. Our numerical resource allows us to calculate the TMI up to the system size $L = 12$ by the methods.

By using the TMI, we can quantify the information spreading and scrambling embedded in the time evolution operator $\hat{U}(t) \equiv e^{-itH}$, where H is either H_{IC} or H_{CS} in this paper. On calculating the TMI, we use the state-channel map that plays an essential role. Under this map, the operator $\hat{U}(t) \equiv e^{-itH}$ is regarded as a pure quantum state in the doubled Hilbert space, $\mathcal{H}_D \equiv \mathcal{H}_{in} \otimes \mathcal{H}_{out}$ [35]. We start from the density matrix at time t, $\rho(t) = \sum_{\nu=1}^{N_D} p_\nu \hat{U}(t)|\nu\rangle\langle\nu|(\hat{U}(t))^\dagger$, where $\{|\nu\rangle\}$ is a set of a orthogonal bases states (time independent), N_D is the dimension of the Hilbert space in the system, and an input ensemble is encoded by parameters $\{p_\nu\}$. Then, by applying the state-channel map to the density matrix $\rho(t)$, the time-evolution operator is mapped into a pure state in the doubled Hilbert space,

$$\rho(t) \to |U(t)\rangle = \sum_\mu \sqrt{p_\nu}(\hat{I} \otimes \hat{U}(t))|\nu\rangle_{in} \otimes |\nu\rangle_{out}, \quad (5)$$

where $\hat{I}$ is the identity operator and $\{|\nu\rangle_{in}\}$ and $\{|\nu\rangle_{out}\}$ are the same set of orthogonal bases state. The time evolution operator $\hat{U}(t)$ acts only on the out orthogonal states $|\nu\rangle_{out}$. An arbitrary input ensemble can be employed by tuning $\{p_\nu\}$ [35]. In this paper, however, we mostly focus on the infinite temperature ensemble, i.e., $p_\nu = 1/N_D$ to see universal properties of the time-evolution unitary. Then, at $t = 0$, as $\hat{U}(0) = \hat{I}$, the in state and out state are maximally entangled. To calculate the TMI under the time evolution with the Hamiltonian H_{IC}/H_{CS}, spatial partitioning of the pure state $|U(t)\rangle$ has to be specified. The spatial partitioning is done for both the $t = 0$ in state and the out state at t, respectively. Figure 3 shows that the $t = 0$ state [given by $\rho(t = 0)$] is divided into two subsystems A and B, and the state at time t [given by $\rho(t)$] is divided into two subsystems C and D. In later calculations, we mostly focus on the partition with the equal length of A and B (and also C and D) subsystems, as well as asymmetric one for specific purposes. (See later discussion.)

Under this spatial partitioning, the density matrix of the pure state $|U(t)\rangle \in \mathcal{H}_D$ is denoted as $\rho_{ABCD}(t) =$

$|U(t)\rangle\langle U(t)|$. From this full density matrix $\rho_{ABCD}(t)$, a reduced density matrix for a subsystem X is obtained by tracing out the degrees of freedom in the complementary subsystem of X denoted by $\bar{X}$, i.e., $\rho_X(t) = \mathrm{tr}_{\bar{X}}\rho_{ABCD}$. From the reduced density matrix $\rho_X(t)$, the operator entanglement entropy (OEE) for the subsystem X is obtained by conventional von-Neumann EE, $S_X = -\mathrm{tr}[\rho_X \log \rho_X]$. From the OEE, we introduce the bipartite mutual information (BMI) of X and Y subsystems (where X, Y are some elements of the set of the subsystems $\{A, B, C, D\}$, and $X \neq Y$):

$$I(X : Y) = S_X + S_Y - S_{XY}. \tag{6}$$

The value of $I(X : Y)$ quantifies how subsystems X and Y correlate with each other.

By using the BMI, the TMI for subsystems A, C, and D is defined as

$$I_3(A : C : D) = I(A : C) + I(A : D) - I(A : CD). \tag{7}$$

The above TMI quantifies how the initial information embedded in the subsystem A spreads into both subsystems C and D in the output state. If the spread of the information in A sufficiently occurs across the entire system at time t, $I_3(t)$ gets a negative value, while the BMI keeps a non-negative value even in such a situation. In general, I_3 is zero at $t = 0$, as $|U(0)\rangle$ is the product state of the EPR pair at each lattice site. When the time-evolution operator acts as a strong scrambler, I_3 acquires a large negative value under the time evolution. On the other hand, if the time evolution operator does not act as an efficient scrambler, I_3 remains small. Hence, I_3 is a good indicator to quantify the degree of scrambling, i.e., the information spreading. In this paper, we mostly employ the TMI to characterize the scrambling for our target models, as well as quench dynamics of the EE.

In the following numerical calculations, it is convenient to set a reference frame of the TMI, I_3, as in Refs. [51,54]. The reference flame is the value of the TMI of the Haar random unitary, I_3^H, which depends on the Hilbert space dimension of the system size L [57]. The value of I_3^H can be numerically calculated [58]. Then, we define a normalized TMI, $\tilde{I}_3(A : C : D)$, as follows:

$$\tilde{I}_3(A : C : D) \equiv \frac{I_3(t)}{I_3^H}. \tag{8}$$

In the following sections, we numerically obtain the value of $\tilde{I}_3$.

Here, some remarks are in order. In the practical calculation, we do not directly obtain the density matrix in the doubled Hilbert space, $\rho_{ABCD}(t)$. Instead, some specific methods are utilized to study systems as large as possible by our numerical resource. Details are explained in our previous paper [55]. In the following numerical calculations, we also employ the Quspin solver [59] to efficiently construct the numerical basis and time evolution operators.

III. NUMERICAL STUDIES

In this section, we shall perform the systematic numerical study by observing the quench dynamics of the EE and the information spreading quantified by the TMI. We show typical dynamical aspects inherent in both systems, H_{IC} and H_{CS}.

The numerical investigation of the models uncovers the initial state dependence of the quench dynamics of the EE, which is strongly related with duality in the random Ising spin chain, and also it clarifies the characteristic behavior of the TMI for systems with topological order. In particular, the calculation of the TMI is independent of the choice of initial state and exploits essential properties of the scrambling embedded in the unitary time-evolution operator: (i) We capture distinct phase transitions and their phase boundary. (ii) By varying the size of the partitioning in the calculation of the TMI, we can extract the bulk structure of information spreading for both topological MBLs, corresponding to the degree of the scrambling. The SG-MBL and CS-MBL phases can be clearly distinguished from this aspect. In what follows, we set a unit of time $\hbar/W$ in numerical calculations of quench dynamics.

A. Quench dynamics of bipartite EE: Random Ising spin chain

We start to show the numerical results of the quench biparite EE of the system H_{IC} at infinite temperature for $g = 0$ and $g = 0.2$. The case of $g = 0$ is the TRIM, and the IRC point at $\delta = 0$ separates the paramagnetic and spin glass localized phases [41]. The ground state for an arbitrary δ is the Griffiths state in which both the typical length and typical timescale have very broad distributions [41–43]. This gapless Griffiths phase persists at finite temperature, as well as the spin-glass order for $\delta \gg 1$. Therefore, it is interesting to see how entanglement spreads in that specific regime. For the case of the interacting case with $g > 0$, on the other hand, the ergodic state intervenes between the two MBL states, which are connected by duality. How the EE spreads in the states connected by duality is an interesting problem and it sheds light on quantum information spreading, as we see later on.

We study the quench dynamics in this subsection, i.e., the time evolution of the half-chain von Neumann entropy, EE(t) obtained from a time-evolved state. We first consider the noninteracting case of the random Ising chain with $g = 0$, the TRIM. The quench half-chain EE, EE(t), is defined as follows:

$$\mathrm{EE}(t) = -\mathrm{Tr}[\rho_{\mathrm{r}}(t) \log(\rho_{\mathrm{r}}(t))], \tag{9}$$

where $\rho_{\mathrm{r}}(t)$ is the reduced density matrix of the half chain at time t. Let us investigate the case in which the employed initial state is $|\uparrow\uparrow\uparrow\cdots\rangle_Z$ in the σ^z basis. The results in Fig. 4 show that EE(t) for $\delta = -4.0$ and -3.0 keeps a very small value during the time evolution, and EE(t) for the other δ's exhibits rather strong oscillating behavior. The averaged values of EE(t) in the central regime of δ are larger than those of $\delta = 4.0$ and 3.0. This *dynamical behavior* obviously reflects the IRC at $\delta = 0$. We observed similar behavior of EE(t) for the initial state $|\uparrow\downarrow\uparrow\downarrow\cdots\rangle_Z$ (not shown). This strong oscillation of EE(t) is an unusual one and is expected to reflect the Griffiths properties of the states. For the case of $\delta = -4.0, -3.0$, the random field dominates the bond coupling, and therefore a phenomenon similar to Anderson localization takes place there with vanishingly small EE(t).

Let us turn to the interacting case with $g = 0.2$. In Figs. 5(a) and 5(b), we display the calculations of EE(t) for the initial states $|\uparrow\uparrow\uparrow\cdots\rangle_Z$ in the σ^z basis and also $|\uparrow\uparrow\uparrow \cdots\rangle_X$ in the σ^x basis, respectively. We first note that the state for $g = 0.2$ does not have the Griffiths-state nature, as EE(t) is
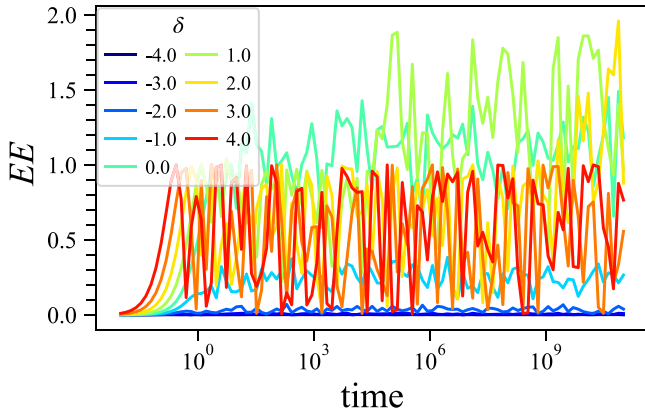
FIG. 4. Quench dynamics of the entanglement entropy, EE(t): The random Ising spin chain, $H_{IC}|_{g=0}$ in Eqs. (1). For $\delta \gg 1$, EE(t) oscillates quite rapidly, whereas for $\delta \ll -1$, it keeps very small values. The system with $\delta = 0$ corresponds to infinite randomness critical point. The system size is $L = 12$.

quite stable compared with the noninteracting case. Figure 5 shows interesting behaviors of EE(t), that is, for the initial state $| \uparrow\uparrow\uparrow \cdots \rangle_Z$, EE($t$) for $\delta = 4.0, 3.0$ acquires large values in the time evolution, whereas for $| \uparrow\uparrow\uparrow \cdots \rangle_X$, EE($t$) for $\delta = -4.0, -3.0$ increases similarly and saturates to large values. This result indicates that the bond coupling, $\sum_i \sigma_i^x \sigma_{i+1}^x$, dominates the field coupling, $\sum_i h_i \sigma_i^z$, for $\delta \gg 1$, and the states $| \uparrow\uparrow\uparrow \cdots \rangle_Z$ contains all states of the σ^x basis, then, as
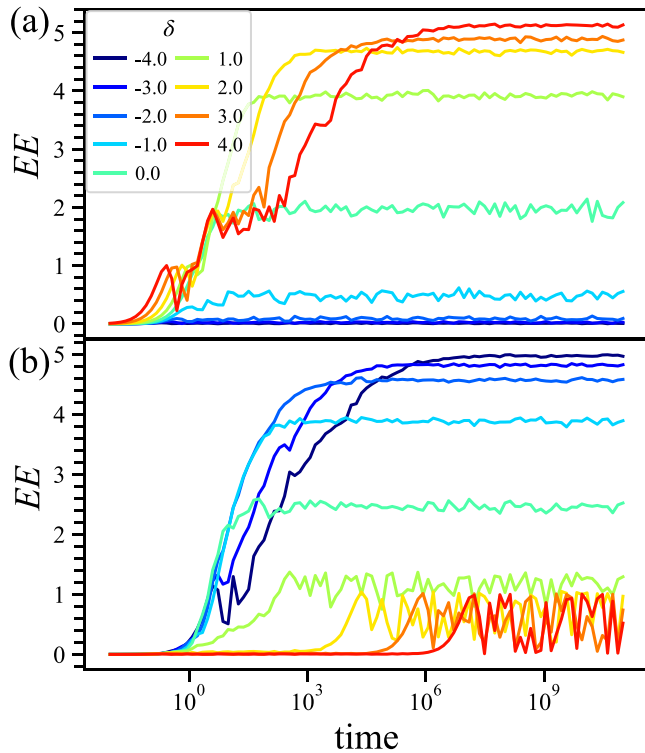

FIG. 5. Quench dynamics of the entanglement entropy, EE(t): the random Ising spin chain with $g = 0.2$ for $L = 12$. (a) Initial state: $|\psi(t = 0)\rangle = | \uparrow\uparrow\uparrow \cdots \rangle_Z$, (b) initial state: $|\psi(t = 0)\rangle = | \uparrow\uparrow\uparrow \cdots \rangle_X = \prod_i \frac{1}{\sqrt{2}}(| \uparrow \rangle_i + | \downarrow \rangle_i)_Z$.

a result, the EE is generated in the time evolution. The same thing happens for the case with $\delta \ll -1$ and $| \uparrow\uparrow\uparrow \cdots \rangle_X$, in which the field coupling dominates the bond coupling. We can understand the above behavior of EE(t) from duality. In the Hamiltonian level, the random parameters $\{J_i\}$ and $\{h_i\}$ are interchanged by Eqs. (2). The above numerical study of EE(t) shows that duality transformation of the initial state is needed for EE(t) to exhibit similar behavior in the corresponding duality counterparts. A careful look at Fig. 5(b) reveals some important aspects of the time evolution of EE(t) besides the above increasing behavior. That is, EE(t) for $\delta = 4.0, 3.0$ and the initial state $| \uparrow\uparrow\uparrow \cdots \rangle_X$ has small but finite values for the late time of the time evolution. On the other hand, EE(t) for $\delta = -4.0, -3.0$ and the initial state $| \uparrow\uparrow\uparrow \cdots \rangle_Z$ in Fig. 5(a) keeps vanishingly small values in the time evolution. This result seems to break duality of the Hamiltonian H_{IC}. We think that this discrepancy comes from the topological order of the SG-MBL, which is observed through the EE in Sec. II, i.e., the topological order exhibits long-range correlations [60] characterized by nonlocal order parameters, such as string order, and it possibly enhances information spreading across the almost entire system compatibly with MBL identified by the return probability, etc. More explicitly in the SG-MBL phase, such a nonlocal order may be construct. That is, we can consider a string operator, given by $\langle \prod_{k=i}^{j-1} \sigma_k^x \sigma_{k+1}^x + \cdots \rangle = \langle \sigma_i^x \sigma_j^x \rangle + \cdots$, as in the CS chain discussed in Sec. II. Please note that the leading terms of the LIOMs are given by the dimer, $\{\sigma_i^x \sigma_{i+1}^x\}$, in the SG-MBL regime. The above observation clarifies the relationship between the spin-glass order and the topological order, i.e., the topological order accompanies the long-range spin-glass correlation described by G_r. The long-range correlation makes a pair of large qubits by $\mathbb{Z}_2$ symmetry, and their mixing emerges in late-time evolution as seen in Fig. 5(b).

To understand the above observation for the EE of the SG-MBL state more concretely, let us consider a four-spin system and divide it into two two-spin subsystems, i.e., A and B subsystems. Then, the initial state corresponding to Fig. 5(b) is given by

$$|\psi_0\rangle = | \uparrow\uparrow\uparrow\uparrow \rangle_X$$
$$= \tfrac{1}{2}[\psi(A, +) + \psi(A, -)][\psi(B, +) + \psi(B, -)],$$
$$(10)$$

where $\psi(A, \pm) = \frac{1}{\sqrt{2}}(| \uparrow\uparrow \rangle_A \pm | \downarrow\downarrow \rangle_A)$ (energy eigenstates of A subsystem expressed in the X basis), and similarly for $\psi(B, \pm)$. In the time evolution, other states such as $| \uparrow\downarrow \rangle_A$ emerge only as a perturbation (by $\{h_i \sigma_i^z\}$) because of the existence of the stabilizer, whose leading terms are given by $\{\sigma_i^x \sigma_{i+1}^x\}$ ($|J_i| \gg |h_i|, g$). Then, by ignoring perturbative states, the system can be regarded as a system of two quantum degrees of freedom with two quantum states for each. EE of this kind of system was studied in Ref. [61]. The interactions between A and B subsystems are given by $J_2 \sigma_2^x \sigma_3^x$ and $g(\sigma_1^x \sigma_3^x + \sigma_2^x \sigma_4^x + \sigma_2^z \sigma_3^z)$. These interactions are invariant under $\mathbb{P}$. Especially, $\sigma_2^x \sigma_3^x$, $\sigma_1^x \sigma_3^x$ and $\sigma_2^x \sigma_4^x$ terms generate mixing between the states $\psi(A, +)\psi(B, +) \leftrightarrow \psi(A, -)\psi(B, -)$ and $\psi(A, +)\psi(B, -) \leftrightarrow \psi(A, -)\psi(B, +)$ as they operate such as $| \uparrow\uparrow \rangle_A | \downarrow\downarrow \rangle_B \rightarrow -| \uparrow\uparrow \rangle_A | \downarrow\downarrow \rangle_B$, etc. (The term $\sigma_2^z \sigma_3^z$ works only as a perturbation as $\{h_i \sigma_i^z\}$.) This mixing obviously

generates an extra time dependence in each of the four terms in Eq. (10) [$\psi(A, +)\psi(B, +), \cdots, \psi(A, -)\psi(B, -)$] and a nontrivial reduced density matrix and, as a result, the oscillating EE emerges [61]. In the original many-body system, the wave functions corresponding to $\psi(A, \pm)$, etc., have a complicated form under the time evolution, and the reduced density matrix ρ_A is of high dimensions. However, we expect that an oscillating behavior originating from the above mechanism persists.

Returning to the SPT order, we note that for $i = 1$ and $j = L$, the string operator essentially measures the correlation between edge operators, $\langle\sigma_1^x\sigma_L^x\rangle$, mentioned in Sec. II. This expression of the string order is obviously a reminiscence of the Stokes theorem by which a magnetic flux piercing a surface is expressed by a line integral of vector potential along the boundary.

In addition, we should remark that duality is explicitly broken at edges in the open-boundary system and, therefore, duality does *not* respect the relation between the bulk and its edges.

In the following subsection, we shall study the TMI. The above observations will shed light on the results of the TMI.

B. Tripartite mutual information: Ising spin chain

In the previous subsection, we studied the bipartite EE, EE(t), for the noninteracting ($g = 0$) as well as the interacting case ($g = 0.2$), and obtained interesting results, in particular, from the viewpoint of duality and SPT order. In this subsection, we shall study the behavior of the TMI under the time evolution. In the practical calculation, the system size is $L = 8$, 10, and 12, and the spin chain is divided into two chains with equal length to compute $I_3(A : B : C)$. In the numerical calculation, we focus on the disorder average of the normalized TMI $\tilde{I}_3$ denoted by $\langle\tilde{I}_3\rangle$.

We study the behavior of the TMI for fixed values of g by varying δ to see how it behaves in the various phases. As we explained in Sec. II, we consider the infinite-temperature ensemble. In Fig. 6, we show the time evolution of the TMI, $\tilde{I}_3$, for the non-interacting and interacting Ising spin chains [H_{IC} in Eqs. (1)] with various values of δ. The two cases exhibit quite different behavior, the strong oscillation in the noninteracting, and stable behavior in the interacting case, although the time average of both of them is rather stable and is an increasing function of time. The strong oscillation of $\tilde{I}_3$ in the noninteracting case comes from the Griffiths nature of the broad distribution of the localization length and typical timescale as the above calculation of EE(t) shows. However, $\tilde{I}_3$ has stable values in the short-period time average, which depends on the parameter δ (not shown). A careful look at the calculations in Fig. 6(a) reveals that $\tilde{I}_3$ increases even after $t = 10^9$, in particular, $\delta = 2.0$ and 2.5. See further late-time calculations in the Appendix, where we show the late-time behavior of $\tilde{I}_3$ for $\delta = 2.0$ and 2.5, and find instability of $\tilde{I}_3$, that is, which does not saturate. However, its system-size dependence is quite stable, and we think that this observation guarantees reliability of the result shown in Fig. 7(a). On the other hand, in the interacting case of $g = 0.2$, $\tilde{I}_3$ is an increase function and saturate into stable values depending on δ after the early-time evolution. In Figs. 7(a) and 7(b), we show the
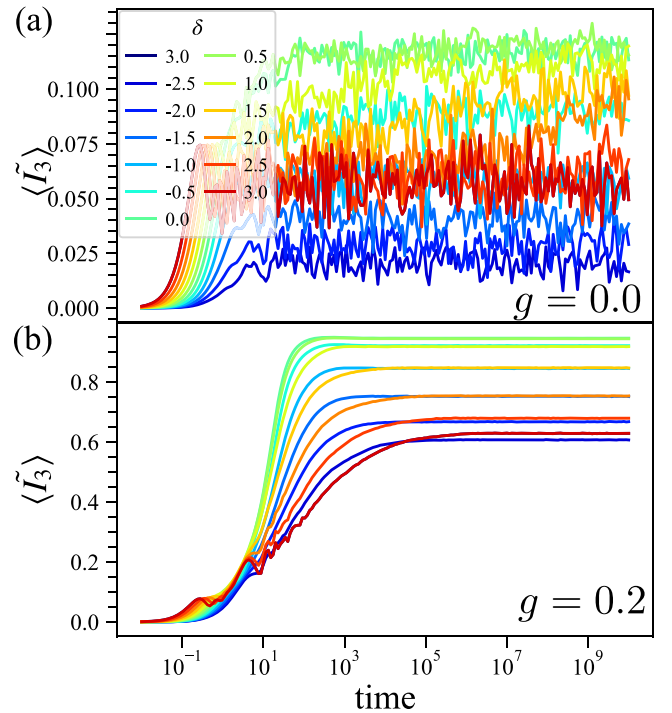

FIG. 6. TMI dynamics of the random Ising spin chain, H_{IC}. (a) The noninteracting case with $g = 0$. The TMI exhibits oscillating behavior for all δ's, but its short-period time average is a stable function of time. (b) The interacting case with $g = 0.2$. After early time increases, the TMI saturates to a finite value for each value of δ. In both cases, the TMI has larger values in the regime $\delta \sim 0$ compared to other regimes. These results were obtained by averaging over the ten disorder realization for the $L = 12$ system. Here, $\langle\cdots\rangle$ denotes disorder average.

saturation values of $\tilde{I}_3$ as a function of δ and also exhibit its system-size dependence for both noninteracting ($g = 0$) and interacting cases ($g = 0.2$). For both cases, $\tilde{I}_3$ has a peak at $\delta = 0$. In the noninteracting case, however, the absolute value of $\tilde{I}_3$ is quite small for the entire parameter regime compared with that in the interacting case. This result obviously corresponds to the phase diagram of the TRIM, in which only the localized phase exists. The state at the IRC point ($\delta = 0$) is recognized as a particular localized state [62], and therefore $\tilde{I}_3$ has a peak at that value. The calculated system-size dependence shows that the curves of $\tilde{I}_3$ do not cross with each other, indicating the nonexistence of phase transitions for the $g = 0$ system besides $\delta = 0$. (However, we shall give a comment on this point at the end of this subsection.)

On the other hand, for the interacting case of $g = 0.2$, $\tilde{I}_3$ in Fig. 7(b) exhibits clear scaling behavior with respect to the system size. The curves of $\tilde{I}_3$ cross with each other at two values of δ, indicating the existence of two phase transitions such as the PM-MBL $\rightarrow$ ETH $\rightarrow$ SG-MBL phases as δ increases. This result is obviously in good agreement with the observation of the half-chain EE in Sec. II. Then, we conclude that the TMI is a good indicator of phase transitions. We have examined $\tilde{I}_3$ for systems of $L = 8$, 10 in addition to $L = 12$ for $g = 0.2$ (not shown) and found that the system-size dependence of the saturation time is rather weak. Then, we
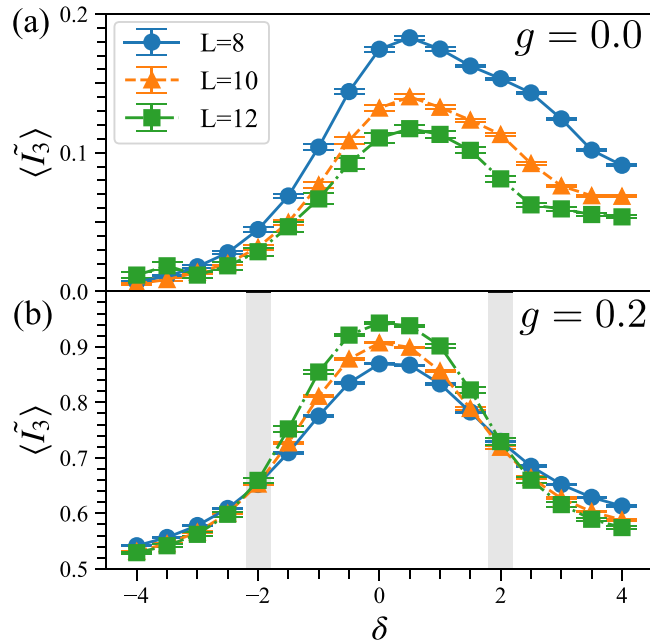
FIG. 7. Saturation values of TMI for various system sizes of random Ising spin chain. (a) $g = 0$ case: $\tilde{I}_3$ exhibits a peak at $\delta = 0$, which corresponds to the infinite random critical point of the random transverse Ising chain. Curves of $\tilde{I}_3$ do not cross with each other, indicating nonexistence of phase transitions besides $\delta = 0$. (b) $g = 0.2$ case: $\tilde{I}_3$ for the interacting case. Curves of $\tilde{I}_3$ cross with each other at the phase transition points, $\delta_{c1} \simeq -\delta_{c2} \simeq -2.0$. Duality symmetry is obviously broken in the MBL regimes. These results were obtained by averaging over 1000, 500, and 100 disorder realizations for $L=8$, 10, and 12 systems. We define saturation values of TMI as the average of $I_3(t)$ at 10 points between $t = 10^9$ and $t = 10^{10}$.

expect that the TMI can be of practical use for large but finite systems.

Interestingly enough, $\tilde{I}_3$ is *not* symmetric under the transformation $\delta \rightarrow -\delta$ outside of the ETH regime, indicating breaking of duality in the localized phases. As discussed in Sec. III A, we think that this discrepancy of duality stems from the SPT order and spatial structure of the stabilizer qubit. Also, we comment that for the SG–MBL limit (for large δ), the background values of TMI seem to exhibit very clear system-size dependence. In fact, we observed the values of I_3/L (*not* $\tilde{I}_3/L$) for the SG–MBL limit are almost independent of the system size (not shown). This behavior also holds for the CS-MBL as we see later, being different from the PM-BML limit with the LIOMs located at a site. Therefore, we expect that this result indicates the existence of bulk size qubits in scrambling process. We will perform a numerical study to verify this expectation in Sec. III D.

Here it is appropriate to comment on the above calculations of the TMI and the static quantities observing localization properties for the $g = 0$ case mentioned in Sec. II A [32]. In Ref. [32], a detailed study on the static half-chain EE and gap ratio for small g indicates that an ergodic phase exists for $-\ln 2 < \delta < \ln 2$ for $g \rightarrow 0$ in the limit $L \rightarrow \infty$. This comes from the avalanche instability of localization [63] in the thermodynamic limit. On the other hand, the TMI in Fig. 7(a) does not exhibit ergodic properties in that parameter region. The
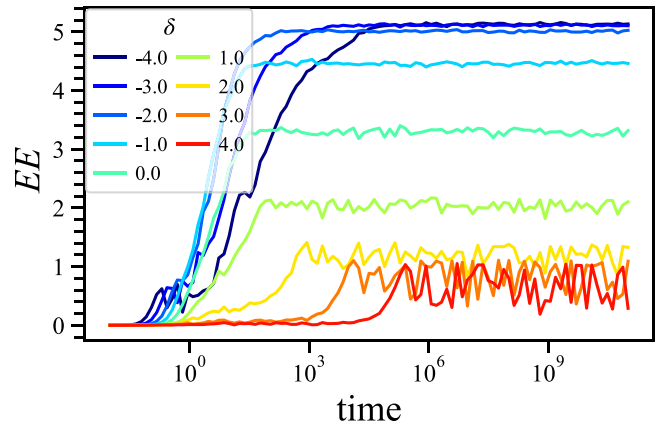

FIG. 8. Quench dynamics of entanglement entropy, EE(t), in the extended cluster-spin model, H_{CS} [Eq. (4)] with $g = 0.2$ and the initial state $| \uparrow\uparrow\uparrow \cdots \rangle_X$. EE($t$) increases quite rapidly for $\delta = -4, -3$ (the CS-MBL regime), whereas it does not for $\delta = 4, 3$ (the SG-MBL regime). The system size is $L = 12$.

obtained results for the interacting case with $g \neq 0$ obviously show that the TMI is a good indicator for localization. However, an apparent discrepancy between the static and dynamic quantities, the TMI, exists for the $g = 0$ case. Unfortunately, we currently do not have a clear understanding of the origin of this discrepancy. One possible origin of this discrepancy is a finite-size effect of the observed TMI and, if so, numerical study of large-scale systems beyond exact diagonalization may be required. We shall give more comments on it at the end of Sec. IV.

C. Quench dynamics of bipartite EE: Cluster spin chain

Let us move onto the numerical study of the model H_{CS} in Eq. (4). We found that there are three phases in the system, i.e., as the value of δ increases, CS-MBL $\rightarrow$ ETH $\rightarrow$ SG-MBL. Both the SG-MBL and CS-MBL are the localized topological phases with distinct topological features, where in the SG-MBL limit, a paired spectrum appears while a quartet spectrum appears in the CS-MBL limit [11,12]. Therefore, it is interesting to see how the TMI behaves in these phases as both SG-MBL and CS-MBL phases have long-range correlations dictated, e.g., by loop orders. Also the spatial structures of the stabilizer in the two MBL regimes for $\delta \rightarrow \pm\infty$ are different. Hence, it is expected that the bulk properties of the information spreading are different in the two phases. In this subsection, we study the quench dynamics of the half-chain EE by varying δ. In Fig. 8, the evolution of the EE, EE(t), is displayed for the initial state $| \uparrow\uparrow\uparrow \cdots \rangle_X$. In particular, we are interested in the difference of EE(t) for the SG-MBL ($\delta \gg 1$) and CS-MBL ($\delta \ll -1$) regimes.

From Fig. 8, it is obvious that the system for $\delta = -3, -4$ exhibits large increases in EE(t), whereas only a small increase for $\delta = 4, 3$ in the time evolution. This behavior obviously comes from the difference of the structures of the stabilizer qubits in these two phases, i.e., the action of the unitary dynamics of $\{\sigma_i^x \sigma_{i+1}^x\}$ in the SG-MBL regime obviously does not induce a significant change of the initial state, i.e., quantum information of the initial state does not scramble significantly. On the other hand, $\{\sigma_i^x \sigma_{i+1}^z \sigma_{i+2}^x\}$ in the CS-MBL
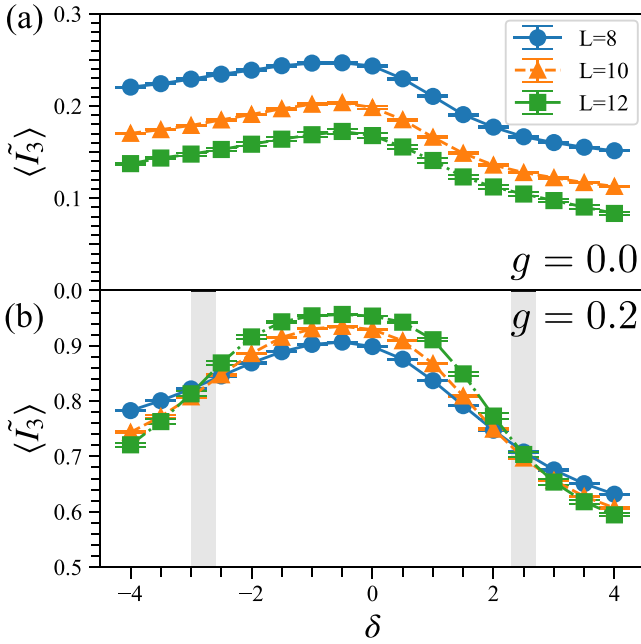
FIG. 9. Saturation values of the TMI for the extended cluster-spin model in Eq. (4) with various system sizes. (a) $g = 0$ case: The data show that $\tilde{I}_3$ is a smooth function of δ, there are no crossings of the curves, and no increase in $\tilde{I}_3$ as L gets larger. These behaviors indicate a direct transition between the SG-MBL and CS-MBL. (b) $g = 0.2$ case: The curves cross with each other at two phase transition points observed by the EE. These results were obtained by averaging over the 1000, 500, and 100 disorder realizations for $L = 8$, 10, and 12 systems.
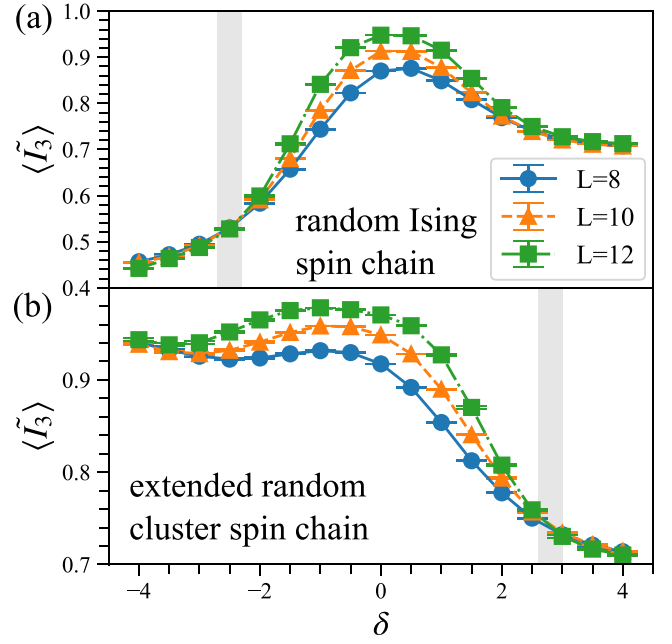

FIG. 10. Saturation values of the TMI for various system sizes under two-site partitioning. (a) Random Ising spin chain for $g = 0.2$. (b) Extended random cluster-spin chain for $g = 0.2$. These results were obtained by averaging over the 1000, 500, and 100 disorder realizations for $L = 8$, 10, and 12 systems.

regime do, as the initial state is strongly scrambled by the above stabilizer qubits. The behavior of EE(t) depends on the interplay of the stabilizer-qubit and initial state.

Here we would like to comment: Which stabilizer, $\{\sigma_i^x \sigma_{i+1}^x\}$ or $\{\sigma_i^x \sigma_{i+1}^z \sigma_{i+2}^x\}$, dominates is automatically determined by parameters of the system under study and the system's location properties in the phase diagram. In other words, study of the phase diagram for the qubit system is required to have stable stabilizers as desired.

In the following subsection, we shall study the TMI, which reflects the nature of the time-evolution unitary itself.

D. Tripartite mutual information: Cluster spin chain

In this subsection, we show the calculations of the TMI, $\tilde{I}_3$, for the CS chain, H_{CS} in Eq. (4). In the numerical calculation, we focus on the disorder average of the normalized TMI $\langle \tilde{I}_3 \rangle$. We observed that $\tilde{I}_3$ has a stable time evolution (not shown), and in Figs. 9(a) and 9(b), we display the saturation values of $\tilde{I}_3$ as a function of δ for various system sizes with the A and B (C and D) $L/2$-chains. As in the random Ising spin chain, the data of $\tilde{I}_3$ for various system sizes indicate the existence of two kinds of phase transitions for the $g = 0.2$ case, as indicated by the calculation of the EE in Sec. II. As in the Ising spin chain, $\tilde{I}_3 \sim 0.6$ in the SG-MBL regime ($\delta \gg 1$). On the other hand, in the CS-MBL ($\delta \ll -1$), $\tilde{I}_3$ has a larger value compared with that value, i.e., $\tilde{I}_3 \sim 0.7$. From the observation obtained in the investigation of the random Ising spin chain, this behavior comes from the difference in the spatial structure

of the stabilizers and the resultant SPT orders. On the other hand, for the $g = 0$ case, the TMI exhibits smooth curves, indicating a direct phase transition between SG-MBL and CS-MBL at least for the small but finite systems.

From the investigation of the TMI given so far, we want to see if there exist some other quantities concerning the TMI, which reflects spatial magnitude of logical (stabilizer) qubits in the MBL states. To this end, we calculate the TMI as varying the size of the subsystem A and D, that is, changing the partitioning of the in and out Hilbert spaces. In particular, we are interested in partitioning with the *two-site A and D* (we denote as $L_A = L_D = 2$) subsystem in Fig. 3.

In Figs. 10(a) and 10(b), we show the numerical calculations $\tilde{I}_3$ for the random Ising spin chain and extended CS models under the above-mentioned two-site partitioning. In the SG-MBL phase of the random Ising spin chain and also the CS-MBL phase in the CS model, $\tilde{I}_3$ has larger values compared to those in the equal-length partition. In particular, in the CS-MBL limit, $\tilde{I}_3$ is an increasing function of $|\delta|$, and $\tilde{I}_3 \simeq 1.0$, indicating *apparent chaotic behavior* of the CS-MBL for two-site partitioning. On the other hand, in the PM-MBL state in Fig. 10(a), $\tilde{I}_3$ is a decreasing function of $|\delta|$. To investigate this peculiar behavior of $\tilde{I}_3$, we calculate $\tilde{I}_3$ for other partitioning such as $L_A = L_D \equiv r = 3, \cdots, L/2 - 1$ for the deep PM-MBL, SG-MBL, and CS-MBL phases. The results are shown in Fig. 11. We readily find that $\tilde{I}_3$ in the PM-MBL is an increasing function of r, indicating that quantum information encoded in subsystem A remains inside of subsystem C until saturation is achieved in the dynamics. Contrary to the above plausible result of the PM-MBL, in SG-MBL and also CS-MBL with SPT order, $\tilde{I}_3$ is a decreasing function of r,
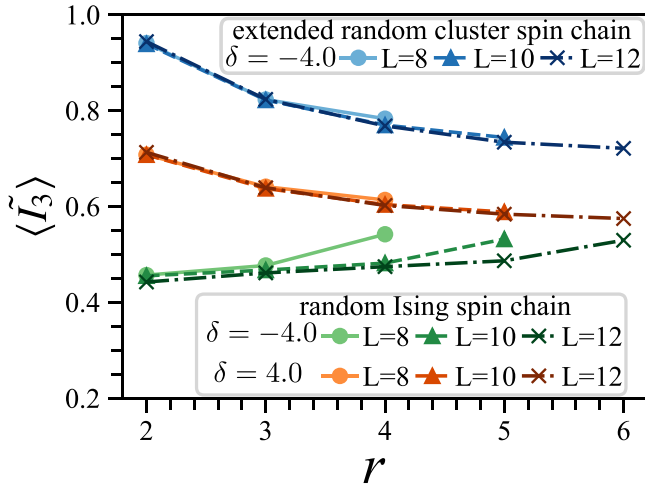
FIG. 11. Saturation values of the TMI for various partitionings of the system. In the PM-MBL, $\tilde{I}_3$ is an increasing function of $r = L_A = L_D$, indicating that quantum information encoded in the initial A system remains in the C subsystem, as expected. On the other hand, for the SG-MBL and CS-MBL with topological order, $\tilde{I}_3$ is a decreasing function of r. This unexpected result comes from a finite spatial magnitude of stabilizer qubit in the topological state.

and this decreasing tendency is stronger in CS-MBL than in SG-MBL.

It is obvious that the above peculiar phenomenon is related to the spatial structure of the stabilizer qubits, i.e., in the deep MBL regime, $\{\sigma_i^x \sigma_{i+1}^x\}$ in SG-MBL and $\{\sigma_i^x \sigma_{i+1}^z \sigma_{i+2}^x\}$ in CS-MBL, is equal to or larger than two-site and also these forms are deformed by the interactions, whereas the stabilizer qubit in the deep PM-MBL is a nearly single spin $\{\sigma_i^z\}$. (For the stabilizer-qubit in the CS-MBL, please see the following analytical discussion.) This fact means that quantum information encoded in a smaller A subsystem than stabilizer qubits *underflows* a stabilizer qubit, as information, which is to be encoded in the stabilizer qubit, is lost by tracing out quantum information in the B subsystem. As a result, $\tilde{I}_3$ exhibits a chaoticlike behavior even in the MBL state. In other words, the above calculation can exhibit spatial magnitude of LIOMs in the MBL regimes. Obviously, the existence of the stable stabilizer qubits with a finite magnitude also supports MBL and the SPT order. Therefore, the present phenomenon is expected to be rather universal.

As one may wonder how the stabilizer qubits (therefore, LIOMs) are deformed (or dressed) by the existence of other terms in the Hamiltonian besides the mutually commuting terms, let us analyze the random CS model in Eq. (4). To this end, it is convenient to introduce the following operators:

$$K_i = \sigma_{i-1}^x \sigma_i^z \sigma_{i+1}^x,$$
$$K_i^{\pm} = \tfrac{1}{2}\big(\sigma_i^x \pm i\sigma_{i-1}^x \sigma_i^y \sigma_{i+1}^x\big), \tag{11}$$

and

$$(K_i^+)^\dagger = K_i^-, \quad (K_i^\pm)^2 = 0, \quad K_i^+ K_i^- + K_i^- K_i^+ = 1,$$
$$K_i^+ K_i^- = \tfrac{1}{2} + \tfrac{1}{2}K_i, \quad [K_i, K_i^\pm] = \pm 2K_i^\pm. \tag{12}$$

Therefore, $K_i^{\pm}$'s are nothing but hard-core bosons and K_i's are their number operators. The leading terms of H_{CS} in Eq. (4), $\{\lambda_i K_i\}$, describe a random potential and $\{\sigma_i^x \sigma_j^x = (K_i^+ + K_i^-)(K_j^+ + K_j^-)\}$ are hopping terms. It is not so difficult to show that the other terms in H_g, $\{\sigma_i^z \sigma_{i+1}^z\}$, describe local interactions between the hard-core bosons. A Majorana representation can be introduced straightforwardly by

$$\chi_i^1 \equiv (K_i^+ + K_i^-), \quad \chi_i^2 \equiv \frac{1}{i}(K_i^+ - K_i^-).$$

By the above observation, the LIOMs are given by $\{K_i\}$'s in the CS-MBL limit, and in the deep MBL regime, the hopping makes $\{K_i\}$'s fluctuate around their original location, and dressed LIOMs are local linear combinations of $\{K_i\}$'s as in Anderson localization. There, weak interactions by the g terms can be treated perturbatively and induce MBL. Investigations on similar situation to the above for spin systems in strong random fields indicates that the LIOMs are well described by dressed spins with a very narrow tail, very close to physical qubits (spins) [64–66]. In the present system, the SPT order exhibits the stability of $\{K_i\}$'s, as the string order is nothing but the expectation value of a product of $\{K_i\}$'s. Furthermore, from the data in Fig. 11, we expect that some fraction of stabilizer qubits have a large-scale cat-state-like nature, which come from the $\mathbb{Z}_2$ symmetry and SPT order and reflect $\tilde{I}_3$ for $r \sim L/2$ in Fig. 11.

IV. DISCUSSION AND CONCLUSION

In this paper, we studied two kinds of quantum spin chains, both of which have a nontrivial phase diagram. By investigating the EE and the order parameters, we first clarified phase diagrams of the random Ising spin chain and extended random CS chain. Then we studied the quench dynamics of the EE for various initial states to obtain an intuitive picture of the quantum information spreading in these systems. We noted the breakdown of duality of the Ising spin chain in the quench dynamics, which gives us a clue to understand how quantum information scrambles. Finally, we calculated the TMI and obtained important perspectives on the information spreading.

The findings which we obtained in this paper are summarized as follows:

(1) To observe the quench dynamics from the view of duality, initial states have to be prepared carefully, as they are connected by duality.

(2) In the time evolution, the EE and TMI exhibit oscillating behavior in the TRIM because of its Griffiths phase character, whereas they become stable by adding interactions H_g in Eqs. (1).

(3) In quench dynamics of the random Ising spin chain, the EE exhibits small but finite breaking of duality.

(4) The above breaking of duality also emerges in the TMI in the MBL regimes.

(5) The TMI exhibits clear system-size dependence and is a good indicator for phase transitions, especially for interacting systems.

(6) The time evolution of the TMI is stable in almost all cases except the Griffiths regime and its saturation values exhibit rather characteristic behavior, in particular, in the partitioning of subsystems with unequal length.

From the above findings obtained by the numerical calculations, we have important insight into how quantum information in the bulk is encoded in quantum spin chains and how randomness (disorder) influences quantum information spreading. Calculation of the TMI in the two-site partitioning of the chain reveals that quantum information is encoded in stabilizer qubits in MBL regimes. We also note that as shown in the numerical result in Fig. 10, the spatial structure of the stabilizer qubit in the MBL regime is robust for (at least) weak interactions. The stabilizer qubits are nothing but the local bits or LIOMs, which were introduced to explain logarithmic time evolution of the quench EE in the MBL regimes. In the ordinary spin chains in random magnetic fields, the local bits are described by dressed Pauli spin operators that substantially reside on a single site in the localization limit. On the other hand, in the present paper, the local bits are explicitly given by the multisite spin composites (stabilizers) such as $\{\sigma_i^x \sigma_{i+1}^x\}$ and $\{\sigma_i^x \sigma_{i+1}^z \sigma_{i+2}^x\}$ in the MBL limit, and it is expected that they are spatially expanded by the additional interactions between spins. Therefore, they behave differently from ordinary local bits because of their spatial magnitude, as explicitly observed by the TMI in the two-site partitioning. In quantum information science, the viewpoint of the spatial structure of stabilizer qubits may be important and useful in constructing practical quantum circuits by using quantum physical devices.

Another interesting observation obtained in this paper concerns the IRC and Griffiths nature of the random Ising spin chain. In the TRIM, almost all quantities observed in this work exhibit unstable behavior in the time evolution. The study of the TRIM has a long history but has not been completed yet. The present paper reveals its peculiar behavior in a quantum information aspect. We think that this finding and detailed study of the TRIM from a quantum information viewpoint will uncover the nature of the IRC and Griffiths phase. This is a future problem.

The above observations clearly indicate that the nature of quantum information scrambling is determined by the phase diagram of the model describing that quantum system, and the stability of the stabilizer can be predicted by the knowledge of the phase diagram. This result may be of great importance for, e.g., constructing logical qubits by means of stabilizer code. How to utilize the knowledge of phase diagrams for construction of logical code, etc. is an interesting future problem. One example in this direction is the random circuit of projective transverse field Ising model studied in Refs. [67–69]. In that system, projective measurements (stabilizers), which are given by $\{\sigma_i^z\}$ and $\{\sigma_i^x \sigma_{i+1}^x\}$ (or $\{\sigma_i^x\}$ and $\{\sigma_i^z \sigma_{i+1}^z\}$), are applied in each time step with probability p and $1 - p$, respectively. It is expected that p plays a role of δ in the random Ising spin chain in this paper, and the random distribution of the stabilizers corresponds to random variables $\{J_i\}$ and $\{h_i\}$. In fact, it was observed that the EE tends to $\log 2$ ($\log 1 = 0$) for the limit $p \to 0$ (1) as in the random Ising spin chain. Furthermore, a phase transition takes place at $p = 0.5$, and the mutual information has a finite value for $p < 0.5$, whereas it vanishes for $p > 0.5$. The phase for $p < 0.5$ is regarded as a spin-glass phase with finite bond percolation. These results obviously coincide with the behavior of SG-MBL and PM-MBL in the random Ising spin chain. A similar projective random circuit system corresponding to the XZZX spin chain

was also studied very recently [70]. Then, it is interesting to study a random circuit of projective measurements corresponding to the extended random CS chain investigated in this paper. This work is in progress. Another direction is to study the relationship between the TMI and more practical information spreading [71], and such an application may be interesting.

We also note that there is a close connection between the present paper and topological Majorana quantum memory [72–74]. Knowledge of stable quantum storing in that system by topologically produced global Bell clusters helps us get an intuitive picture of the significantly large TMI in the SG-MBL and CS-MBL regimes. Detailed study on the relation is a future work.

Finally, we would like to comment on recent studies on MBL transitions in the thermodynamic limit [75–77]. These works indicate that putative MBL, which is observed in finite systems, cannot survive in the thermodynamic limit. An idea called a finite-size MBL regime was proposed, which is to be distinguished from the genuine MBL phase. Most studies focused on XXZ and XXX spin models in a random external field, and therefore the investigation of the TMI for the XXX spin model in Ref. [54] is quite useful. There, the behavior of the TMI was studied by the exact diagonalization in small systems, and exhibits a phase-transition-like behavior with a critical magnitude of the random field, which is close to the ones obtained by the gap ratio and the half-chain EE. This indicates that the MBL phase transition observed by the TMI may correspond to the finite-size MBL regime. The phase transitions observed in this work may be a crossover to the finite-size MBL regime, in particular, the SPT nature protected by MBL may disappear in the thermodynamic limit. However, from the quantum information point of view,
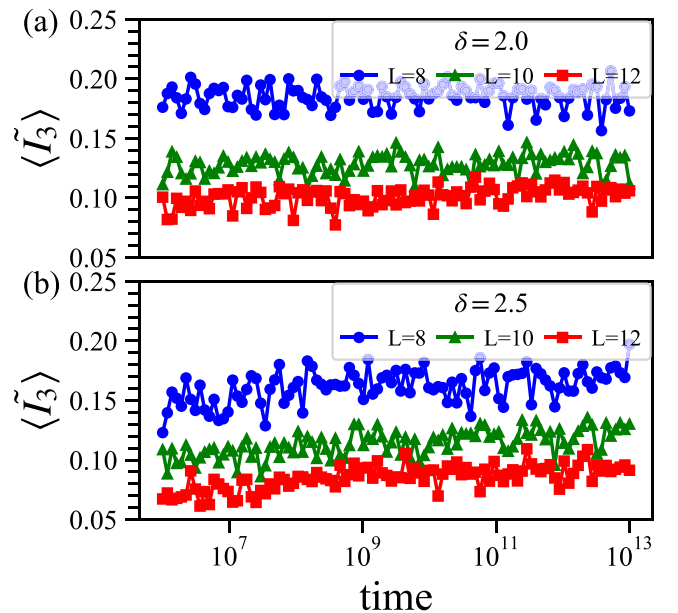

FIG. 12. TMI dynamics of random Ising chain ($g = 0$) with various system sizes in the long-time limit: (a) $\delta = 2.0$ and (b) $\delta = 2.5$. We employ the same random coefficients J_i and h_i of Fig. 6 and take the same disorder averages.

our findings in the present paper are useful, as devices in quantum-information instruments are of finite size and a period using them is also finite. Our paper clarified the parameter regimes in which relevant states emerge and are stable and gives guides for constructing quantum networks using many-body spins such as described by CS models.

ACKNOWLEDGMENTS

APPENDIX: NUMERICAL VALIDITY OF THE SATURATION VALUE OF THE TMI

In this paper, we have found that the saturation value of the $\tilde{I}_3$ distinguishes the phases. However, in Fig. 6, one can see $\tilde{I}_3$ with $\delta = 2.0$ and 2.5 do not seem to reach the saturation values. In this Appendix, we verify that such a weakly increasing nature of $\tilde{I}_3$ does not affect the main results. Figure 12 shows $\tilde{I}_3$ dynamics in the further long time period up to $t = 10^{13}$ with the same numerical conditions as Fig. 6. $\tilde{I}_3$ may increase with time evolution; however, as the system size L increases, $\tilde{I}_3$ decreases, which implies the absence of the crossing for $\tilde{I}_3$, i.e., a weak increase in $\tilde{I}_3$ does not affect the main results.

[1] R. Nandkishore and D. A. Huse, Annu. Rev. Condens. Matter Phys. **6**, 15 (2015).

[2] D. A. Abanin and Z. Papić, Ann. Phys. **529**, 1700169 (2017).

[3] F. Alet and N. Laflorencie, C. R. Phys. **19**, 498 (2018).

[4] D. A. Abanin, E. Altman, I. Bloch, and M. Serbyn, Rev. Mod. Phys. **91**, 021001 (2019).

[5] V. Khemani, S. P. Lim, D. N. Sheng, and D. A. Huse, Phys. Rev. X **7**, 021013 (2017).

[6] M. Žnidarič, T. Prosen, and P. Prelovšek, Phys. Rev. B **77**, 064426 (2008).

[7] J. H. Bardarson, F. Pollmann, and J. E. Moore, Phys. Rev. Lett. **109**, 017202 (2012).

[8] D. A. Huse, R. Nandkishore, V. Oganesyan, A. Pal, and S. L. Sondhi, Phys. Rev. B **88**, 014206 (2013).

[9] J. A. Kjäll, J. H. Bardarson, and F. Pollmann, Phys. Rev. Lett. **113**, 107204 (2014).

[10] S. Iyer, V. Oganesyan, G. Refael, and D. A. Huse, Phys. Rev. B **87**, 134202 (2013).

[11] Y. Bahri, R. Vosk, E. Altman, and A. Vishwanath, Nat. Commun. **6**, 7341 (2015).

[12] K. S. C. Decker, D. M. Kennes, J. Eisert, and C. Karrasch, Phys. Rev. B **101**, 014208 (2020).

[13] R. Sahay, F. Machado, B. Ye, C. R. Laumann, and N. Y. Yao, Phys. Rev. Lett. **126**, 100604 (2021).

[14] A. Smith, J. Knolle, D. L. Kovrizhin, and R. Moessner, Phys. Rev. Lett. **118**, 266601 (2017).

[15] A. Smith, J. Knolle, R. Moessner, and D. L. Kovrizhin, Phys. Rev. B **97**, 245137 (2018).

[16] J. Park, Y. Kuno, and I. Ichinose, Phys. Rev. A **100**, 013629 (2019).

[17] M. Schulz, C. A. Hooley, R. Moessner, and F. Pollmann, Phys. Rev. Lett. **122**, 040606 (2019).

[18] E. van Nieuwenburg, Y. Baum, and G. Refael, Proc. Natl. Acad. Sci. **116**, 9269 (2019).

[19] T. Orito, Y. Kuno, and I. Ichinose, Phys. Rev. B **101**, 224308 (2020).

[20] Y. Kuno, T. Orito, and I. Ichinose, New J. Phys. **22**, 013032 (2020).

[21] C. Danieli, A. Andreanov, and S. Flach, Phys. Rev. B **102**, 041116(R) (2020).

[22] N. Roy, A. Ramachandran, and A. Sharma, Phys. Rev. Res. **2**, 043395 (2020).

[23] J. Zurita, C. E. Creffield, and G. Platero, Adv. Quantum Technol. **3**, 1900105 (2020).

[24] C. Danieli, A. Andreanov, T. Mithun, and S. Flach, Phys. Rev. B **104**, 085131 (2021).

[25] C. Danieli, A. Andreanov, T. Mithun, and S. Flach, Phys. Rev. B **104**, 085132 (2021).

[26] T. Orito, Y. Kuno, and I. Ichinose, Phys. Rev. B **103**, L060301 (2021).

[27] T. Orito, Y. Kuno, and I. Ichinose, Phys. Rev. B **104**, 094202 (2021).

[28] H. J. Briegel and R. Raussendorf, Phys. Rev. Lett. **86**, 910 (2001).

[29] W. Son, L. Amico, R. Fazio, A. Hamma, S. Pascazio, and V. Vedral, Europhys. Lett. **95**, 50001 (2011).

[30] P. Smacchia, L. Amico, P. Facchi, R. Fazio, G. Florio, S. Pascazio, and V. Vedral, Phys. Rev. A **84**, 022304 (2011).

[31] T. B. Wahl and B. Béri, Phys. Rev. Res. **2**, 033099 (2020).

[32] N. Laflorencie, G. Lemarié, and N. Macé, Phys. Rev. Res. **4**, L032016 (2022).

[33] T. B. Wahl, F. Venn, and B. Béri, Phys. Rev. B **105**, 144205 (2022).

[34] S. Moudgalya, D. A. Huse, and V. Khemani, arXiv:2008.09113.

[35] P. Hosur, X.-L. Qi, D. A. Roberts, and B. Yoshida, J. High Energy Phys. 02 (2016) 004.

[36] S. H. Shenker and D. Stanford, J. High Energy Phys. 03 (2014) 067.

[37] J. Maldacena, S. H. Shenker, and D. Stanford, J. High Energy Phys. 08 (2016) 106.

[38] B. Swingle and D. Chowdhury, Phys. Rev. B **95**, 060201(R) (2017).

[39] R. Q. He and Z. Y. Lu, Phys. Rev. B **95**, 054201 (2017).

[40] S. Sahu, S. Xu, and B. Swingle, Phys. Rev. Lett. **123**, 165902 (2019).

[41] D. S. Fisher, Phys. Rev. B **51**, 6411 (1995).

[42] A. P. Young and H. Rieger, Phys. Rev. B **53**, 8486 (1996).

[43] D. S. Fisher, Physica A **263**, 222 (1999).

[44] B. Zeng and D. L. Zhou, Europhys. Lett. **113**, 56001 (2016).

[45] P. Fendley, J. Stat. Mech.: Theory Exp. (2012) P11020.

[46] J. Kemp, N. Y. Yao, C. R. Laumann, and P. Fendley, J. Stat. Mech.: Theory Exp. (2017) 063105.

[47] N. M. Gergs, L. Fritz, and D. Schuricht, Phys. Rev. B **93**, 075129 (2016).

[48] H. Tasaki, *Physics and Mathematics of Quantum Many-Body Systems*, Graduate Texts in Physics (Springer International Publishing, Cham, 2020).

[49] S. Lieu, D. K. K. Lee, and J. Knolle, Phys. Rev. B **98**, 134507 (2018).

[50] Y. Kuno, T. Orito, and I. Ichinose, New J. Phys. **24**, 073019 (2022).

[51] O. Schnaack, N. Bölter, S. Paeckel, S. R. Manmana, S. Kehrein, and M. Schmitt, Phys. Rev. B **100**, 224302 (2019).

[52] E. Mascot, M. Nozaki, and M. Tezuka, arXiv:2012.14609 (2020).

[53] I. MacCormack, M. T. Tan, J. Kudler-Flam, and S. Ryu, Phys. Rev. B **104**, 214202 (2021).

[54] N. Bölter and S. Kehrein, Phys. Rev. B **105**, 104202 (2022).

[55] Y. Kuno, T. Orito, and I. Ichinose, Phys. Rev. A **106**, 012435 (2022).

[56] A. Zabalo, M. J. Gullans, J. H. Wilson, S. Gopalakrishnan, D. A. Huse, and J. H. Pixley, Phys. Rev. B **101**, 060301(R) (2020).

[57] I_3^H is calculated under the dimension 2^L including full sectors of total magnetization.

[58] When all the subsystems are the same length, the values of I_3^H/L are -0.820539, -0.855923, and -0.879814 for $L = 8$, 10, and 12. When the length of subsystems A and D are 2 and subsystems B and C are $L - 2$, the values of I_3^H are -3.3060497, -3.309270, and -3.308958 for $L = 8$, 10, and 12.

[59] We employed the Quspin solver for all numerical calculations: P. Weinberg and M. Bukov, SciPost Phys. **7**, 020 (2019); **2**, 003 (2017).

[60] We note that this statement does not necessarily mean the SG-MBL and CS-MBL phases are long-range entangled phases.

[61] M. Serbyn, Z. Papić, and D. A. Abanin, Phys. Rev. Lett. **110**, 260601 (2013).

[62] I. A. Kovács, T. Pető, and F. Iglói, Phys. Rev. Res. **3**, 033140 (2021)

[63] W. De Roeck and F. Huveneers, Phys. Rev. B **95**, 155129 (2017).

[64] A. Chandran, I. H. Kim, G. Vidal, and D. A. Abanin, Phys. Rev. B **91**, 085425 (2015).

[65] S. Bera, T. Martynec, H. Schomerus, F. Heidrich-Meisner, and J. H. Bardarson, Ann. Phys. **529**, 1600356 (2017).

[66] T. Orito, Y. Kuno, and I. Ichinose, Phys. Rev. B **105**, 094201 (2022).

[67] N. Lang and H. P. Büchler, Phys. Rev. B **102**, 094204 (2020).

[68] S. Sang and T. H. Hsieh, Phys. Rev. Res. **3**, 023200 (2021).

[69] Y. Li and M. P. A. Fisher, arXiv:2108.04274.

[70] K. Klocke and M. Buchhold, arXiv:2204.08489.

[71] S. Ashhab, Phys. Rev. A **92**, 062305 (2015)

[72] A. Y. Kitaev, Phys.-Usp. **44**, 131 (2001).

[73] S. Bravyi, B. M. Terhal, and B. Leemhuis, New J. Phys. **12**, 083039 (2010).

[74] A. Nahum and B. Skinner, Phys. Rev. Res. **2**, 023288 (2020).

[75] D. Sels and A. Polkovnikov, Phys. Rev. E **104**, 054105 (2021).

[76] A. Morningstar, L. Colmenarez, V. Khemani, D. J. Luitz, and D. A. Huse, Phys. Rev. B **105**, 174205 (2022).

[77] D. Sels, Phys. Rev. B **106**, L020202 (2022).

Both phases are symmetry-protected topological phases with localization nature, that is, each static eigenstate is short-range entangled, which obeys area law.